

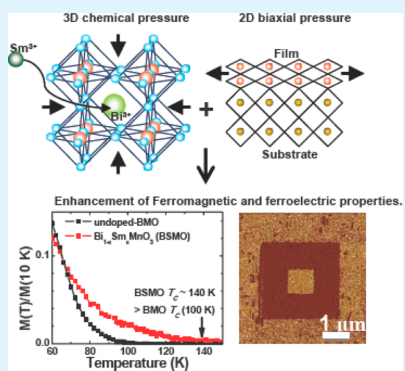
Ferroelectric Sm-Doped BiMnO_3 Thin Films with Ferromagnetic Transition Temperature Enhanced to 140 K

Eun-Mi Choi,^{*,†} Ahmed Kursumovic,[†] Oon Jew Lee,[†] Josée E. Kleibeuker,[†] Aiping Chen,[‡] Wenrui Zhang,[‡] Haiyan Wang,[‡] and Judith L. MacManus-Driscoll[†]

[†]Department of Materials Science, University of Cambridge, 27 Charles Babbage Road, Cambridge, CB3 0FS, U.K.

[‡]Department of Electrical and Computer Engineering, Texas A&M University, College Station, Texas 77843-3128, United States

ABSTRACT: A combined chemical pressure and substrate biaxial pressure crystal engineering approach was demonstrated for producing highly epitaxial Sm-doped BiMnO_3 (BSMO) films on SrTiO_3 single crystal substrates, with enhanced magnetic transition temperatures, T_C up to as high as 140 K, 40 K higher than that for standard BiMnO_3 (BMO) films. Strong room temperature ferroelectricity with piezoresponse amplitude, $d_{33} = 10 \text{ pm/V}$, and long-term retention of polarization were also observed. Furthermore, the BSMO films were much easier to grow than pure BMO films, with excellent phase purity over a wide growth window. The work represents a very effective way to independently control strain *in-plane* and *out-of-plane*, which is important not just for BMO but for controlling the properties of many other strongly correlated oxides.



KEYWORDS: BiMnO_3 , multiferroic, film, PLD

1. INTRODUCTION

Multiferroic materials have attracted wide interest due to their promising practical applications based on the coexistence of magnetism and ferroelectricity, the coupling which gives rise to magnetoelectricity (ME) (or ferroelectromagnetism).^{1–4} With these materials, there is the possibility of creating new kinds of low energy computer memory. However, to date, no ferromagnetic ferroelectric material has been reported which operates at near room temperature (RT).

Within single-phase multiferroic materials, BiMnO_3 (BMO) has been extensively investigated because among the many transition metal perovskites which are ferroelectric, BMO is rare as it also is a ferromagnetic (FM) material (maximum reported magnetic transition temperature, T_C , is ~ 100 K).^{5,6} More recent theoretical and experimental results show bulk BMO has a centrosymmetric monoclinic structure ($C2/c$), which means the ground state of BMO is not ferroelectric (FE).⁷ However, in bulk BMO the ferroelectric transition temperature T_{FE} is measured to be ~ 400 K, although saturation polarization is low, only $0.1 \mu\text{C}/\text{cm}^2$ (at ~ 90 K).^{5,6} FE has also been reported in films with $P_r \sim 23 \mu\text{C}/\text{cm}^2$ at 5 K, but here, the FM transition temperature ($T_C \sim 85$ K) and magnetic moment (M) are reduced.⁷ Solovyev et al. proposed that hidden antiferromagnetic (AFM) ordering is responsible for ferroelectricity.⁸

The highly distorted monoclinic structure of BMO which results from the $6s^2$ lone pair character of Bi^{3+} means that the MnO_6 octahedra have a much higher Jahn-Teller (JT) structural distortion (JT distortion parameter $\Delta = (1/6) \sum_{n=1,6} [(d_n - \langle d \rangle)/\langle d \rangle]^2$ of 37.2×10^{-4} and 51.3×10^{-4} , where

$\langle d \rangle$ is the average of the $\langle \text{Mn}-\text{O} \rangle$ bond length) than, for example, A-type AFM LaMnO_3 (31.8×10^{-4}).^{9–11} This gives rise to small $\text{Mn}^{3+}-\text{O}-\text{Mn}^{3+}$ bond angles of $140\text{--}160^\circ$, significantly smaller than the ideal 180° for strong superexchange interaction.⁸ Also, this distortion breaks the degeneracy of the e_g orbital and leads to the three-dimensional (3D) FM superexchange coupling. Two of the three $\text{Mn}^{3+}-\text{O}-\text{Mn}^{3+}$ orbital orderings exhibit FM interactions with one FM interaction along the c -axis (out-of-plane) and both an FM interaction and an AFM interaction in the ab -plane (in-plane).^{11–14} Overall, long-range FM coupling dominates over AFM coupling.¹²

The 3D magnetic state of BMO is very sensitive to changes in bond angle and length by internal and external pressures.^{11,13–16} When high hydrostatic external pressure (>1 GPa) is applied to bulk BMO, there is coexistence of both FM ($T_C = 95$ K, reduced slightly from the T_C of 100 K for the phase under ambient pressure) and AFM ($T_N = 90$ K), despite only producing small changes to the $\text{Mn}^{3+}-\text{O}-\text{Mn}^{3+}$ bond angles (by $\sim \pm 1^\circ$).¹¹

High temperatures and pressures of 1100 K and 6 GPa, respectively, are required to synthesize pure bulk BMO because $\text{Bi}_{12}\text{MnO}_{20}$ and $\text{Bi}_2\text{Mn}_4\text{O}_{10}$ compounds are much more stable than perovskite BMO under ambient pressure.^{17,18} In the high pressure bulk phase, the structure is $C2/c$, and FM ordering

Received: March 6, 2014

Accepted: August 20, 2014

Published: August 20, 2014

occurs with a T_C of ~ 100 K (saturation magnetic moment, M_S , of $3.6 \mu_B/\text{Mn}$).

It is possible to make FM BMO thin films of a few 10s nm thickness using the epitaxial strain from the substrate as an effective substitute for high pressure.¹⁹ However, because the monoclinic structure is mismatched to available (pseudo)cubic single crystal substrates, the bulk magnetic moments and T_C are significantly reduced.⁷ The properties of the films depend sensitively on the particular substrate. A T_C of 50 K has been measured on (001) LaAlO₃ (lattice mismatch of -4.3%), 80–100 K on (001) STO (lattice mismatch $<\sim -1\%$), and 100 K on (110) DyScO₃ (lattice mismatch of -0.15%).^{20–22} The films on DyScO₃ were very thin (<10 nm) to give the required coherent strain. From X-ray magnetic circular dichroism (XMCD) measurements, films of DyScO₃ gave M_S up to $3.2 \mu_B/\text{Mn}$ at 8 K and 2 T, and piezoresponse was also observed at RT.²² The results are encouraging but need to be translated to thicker films. So far, however, in films above 30 nm thickness, when the FM properties are optimized, e.g., M_S up to $1.87 \mu_B/\text{Mn}$ ($0.52 M_S$ of bulk) and T_C of 100 K, FE is not achieved.^{5,21} Conversely, in films where FE is observed, they have a reduced M ($0.7 \mu_B/\text{Mn}$ at 10 K and 1 T) and reduced T_C (<90 K).^{23–26}

It is clear that optimization of the individual FM or FE properties is nontrivial; ergo optimization of these two properties simultaneously is compoundedly difficult. However, it is certain that structural straining represents an effective means to tune properties. Both thin film epitaxial strain and chemical pressure strain can be used. A few groups have studied doping of the Bi³⁺ site with La³⁺.^{27–29} So far, this light substitution (La³⁺ has an ionic radius of 1.22 \AA , compared to 1.24 \AA of Bi³⁺ for 9-fold coordination) has meant the films are easier to grow owing to the lower structural distortion. However, La³⁺ substitution has also caused a slight reduction of the JT distortion and consequently weaker FM properties ($T_C \sim 90$ K instead of 100 K for bulk BMO).^{28–31}

The aim of this study is to combine both internal 3D chemical pressure and external 2D biaxial epitaxial pressure in order to independently tune the out-of-plane and in-plane bond lengths. By shrinking the out-of-plane $\langle \text{Mn}–\text{O} \rangle$ FM bonds without also reducing the in-plane $\langle \text{Mn}–\text{O} \rangle$ AFM bonds, there is the possibility to increase the FM coupling in the system and, with it, enhance T_C . Therefore, the idea is to simultaneously undertake (a) epitaxial growth to fix the in-plane lattice parameter to the substrate lattice parameter, i.e., to SrTiO₃ (STO), with $a = 3.905 \text{ \AA}$, which is larger than the expected bulk Bi_{1-x}Sm_xMnO₃ (BSMO) lattice parameter. It would be expected that this should minimize the in-plane AF coupling; and (b) A-site doping with a cation that has a smaller ionic radius than Bi³⁺ and a large JT distortion parameter than Bi³⁺ to reduce the overall cell volume and hence also the out-of-plane $\langle \text{Mn}–\text{O} \rangle$ bond length to optimize the out-of-plane FM coupling.

Our method is very different from a simple chemical substitution of bulk material where the chemical pressure is isostatic, and the $\langle \text{Mn}–\text{O} \rangle$ bond lengths would be reduced in all directions. In that case, while the FM coupling would be increased out-of-plane, the AFM coupling would also be increased in-plane and would likely dominate the magnetic properties owing to the great sensitivity of superexchange coupling to bond length and angle.^{14–16}

The smaller A-site ion dopant used was Sm³⁺ (ionic radius = 1.13 \AA compared to Bi³⁺ = 1.22 \AA).³² SmMnO₃ has a very large JT distortion parameter ($\Delta \sim 50 \times 10^{-4}$), which is close to the

JT distortion of BMO ($\Delta = 37.2 \times 10^{-4}$ and 51.3×10^{-4}).^{9,33} Therefore, Sm substitution is not expected to reduce the JT effect of BMO.

A nominal doping level of 15% was used, i.e., $x = 0.15$ in Bi_{1-x}Sm_xMnO₃ (BSMO). This doping level is not too high to significantly reduce the Bi content and the important 6s² loan pair effect but at the same time is high enough to cause a measurable cell volume reduction. From the ferroelectric point of view, previous results in the related compound BiFeO₃ (Mn and Fe being adjacent in the periodic table) show that Sm doping up to 15% improves the FE.^{34–37}

We found that in films of up to 200 nm thickness, the FM T_C is enhanced to up to 140 K compared to 100 K for the best thin BMO films reported previously. At the same time, strong FE at room temperature was measured with a piezoresponse amplitude (d_{33}) value of 10 pm/V , which is higher than the highest value reported previously for 30 nm thick Bi_{0.9}La_{0.1}MnO₃ (BLMO) films, 2 pm/V at RT.²⁸ Furthermore, we found that films can be readily grown to be phase pure with excellent epitaxy over a wide growth window, which is not the case for undoped BMO.¹⁹

2. EXPERIMENTAL SECTION

Undoped-BMO and BSMO films of 120–200 nm thickness were grown on (001) STO and Nb-SrTiO₃ (Nb-STO) substrates by pulsed laser deposition (PLD). Ceramic targets for the PLD deposition were prepared by thoroughly mixing stoichiometric amounts of Mn₂O₃ and Sm₂O₃ powders, the Bi₂O₃ powder being 10% in excess to counteract Bi evaporation during growth. After mixing, the powders were uniaxially pressed into 1" targets and sintered at 870 °C for 15 h. For the film growth, the laser pulse rate was 2 Hz, and the laser fluence was 1.3 J cm^{-2} . The oxygen pressure was fixed at 100 mTorr. The optimum growth temperature was found to be 650 °C. However, it was possible to grow phase pure films within a temperature window of 630–700 °C.

To confirm the phase purity, crystalline quality, and 3D strain state of the films at room temperature, θ – 2θ scans and reciprocal space maps (RSMs) were carried out using a Panalytical Empyrean high resolution X-ray diffraction (XRD) system. We determined the out-of-plane lattice parameter by averaging the higher angle peaks from θ – 2θ scans, namely, (003) and (004), and the (103) peak in the RSMs. We determined the in-plane lattice parameters also from the (103) peak in RSMs.

To determine film surface morphology, atomic force microscopy (AFM) was performed. The detailed atomic structure was probed by high resolution transmission electron microscopy (HRTEM, JEOL 2010 microscope operating at 200 kV and a JEOL 4000 EX microscope operating at 400 kV). Magnetization measurements ($M - T$ and $M - H$) were made using a superconducting quantum interference device (SQUID) magnetometer (Quantum Design, MPMS). The magnetic moment was converted from emu/cc to μ_B/Mn by using the unit cell volume revealed from XRD and film volume determined by X-ray reflectivity.

Piezoresponse force microscopy (PFM) measurements were performed using an Agilent 5500 scanning probe microscope (Agilent SPM 5500) in PFM mode with 3 (MAC-3) lock-in amplifiers (LIAs) at room temperature. For the PFM measurements, an Olympus Pt-coated tip (Asylum Research AC240TM) was used at an excitation frequency of 15 kHz with an alternating current (AC) voltage V_{AC} of 2 V, polarized by a direct current (DC) bias of V_{DC} of ± 5 V. The inverse (also called converse) piezoelectric effect was used to induce longitudinal (thickness) film displacements on a local scale and beneath the Pt surface electrodes (of $\sim 250 \mu\text{m}$ in diameter). The PFM displacement was influenced little by the electrostatic force between the sample and the cantilever assembly since they were at the same electrical (the whole cantilever body was electrically screened by the tip) and contact (Pt-tip and Pt-patch) potential.³⁸

Table 1. Crystal Structures, Ionic Radii of A-Site ($\langle r_A \rangle$), Cell Parameters, Unit Cell Volume, Magnetic Transition Temperature (T_C), Magnetic Moments (M), and Piezoresponse Amplitude (d_{33}) Comparing BMO of Different Forms and Doping

composition	crystal structure	$\langle r_A \rangle$ [Å] ^a	lattice parameter (Å) of perovskite unit cell		pseudocubic unit cell volume [Å ³]	T_C [K]	M [μ_B/Mn] 1 T	10 K and 1 T	d_{33} [pm/V] RT
			in-plane	out-of-plane					
Bulk Crystals									
BMO ^b	rhombohedral	1.240	3.935	3.989	61.50	105	3.51 (5 K)		
STO ^c	cubic	1.440	3.905	3.905	59.55				
Thin Films on STO									
undoped-BMO (this work)	(pseudo-) tetragonal	1.240	3.90 ± 0.01	3.98 ± 0.01	60.5 ± 0.2	100	0.38		
BSMO (this work)	(pseudo-) tetragonal	1.224	3.90 ± 0.01	3.87 ± 0.01	58.8 ± 0.2	140	1.04		10
BLMO ^d	(pseudo-) tetragonal	1.238	3.905	3.94	60.1	90	1		2

^aAveraged ionic radii of A-site.^{32,41} ^bBulk BMO synthesized at 4 GPa and 600 °C.³⁹ ^cSTO lattice parameter.⁴⁰ ^dBLMO films are 30 nm thick, and the BMO and BSMO films of this work are 200 nm thick.^{28,29}

3. RESULTS AND DISCUSSION

Table 1 shows an overview of structural and physical properties of the 200 nm thick BSMO and undoped-BMO films of this work, compared to BLMO films grown on STO.^{28,29} The BLMO films are good comparator samples because they exhibit good magnetic properties and FE at RT with reasonable sample thickness, (i.e., not too thin; they are ~30 nm), and with lattice parameter information reported. For further reference, bulk BMO made under high pressure and STO are included.^{39,40}

All of the films in Table 1, whether doped or undoped, are tetragonal or pseudotetragonal owing to epitaxial constraints of growth on STO. The cell volume of the BLMO films are similar to our undoped-BMO films, as expected considering the similar sizes of La³⁺ and Bi³⁺. The cell volume for the BSMO films are markedly reduced, namely, 58.8 ± 0.2 Å³ compared to 60.1–60.5 Å³ for the BLMO and BMO films, respectively, consistent with the smaller Sm³⁺ ion size than La³⁺ or Bi³⁺.

Figure 1a shows θ –2θ XRD patterns (logarithmic scale on y-axis) of a 200 nm BSMO film and an undoped-BMO film of the same thickness. In the undoped-BMO film, there are various Bi-rich and Mn-rich secondary phases including α - and β -Bi₂O₃ and (00l) oriented Mn₃O₄. The result confirms literature reports that undoped-BMO films are hard to grow phase pure.¹⁹ However, the BSMO film shows clear peaks of (00l) BSMO and little or no secondary phases indicative of the strong stabilizing effect of Sm on the BMO phase, as discussed later.

To explore the 3D strain state in both the BMO and BSMO films, RSMs around STO (103) were conducted (Figure 1b). The H_{00} value for both undoped-BMO and BSMO are, within error range, equal to the H_{00} value of the STO substrate, indicating full external 2D biaxial epitaxial pressurization of both films. In addition, the out-of-plane d -spacing, revealed from the θ –2θ scan and the RSM, gives an idea of the applied 3D chemical pressure. For BMO, the out-of-plane lattice parameter was found to be 3.98 ± 0.01 Å, which is significantly larger than STO (3.905 Å). By replacing Bi by Sm, the out-of-plane lattice parameter of the (002) diffraction peak of BSMO was reduced to 3.87 ± 0.01 Å. In other words, Sm doping caused a shrinkage of 3% of the out-of-plane lattice parameter when compared to that of the undoped-BMO film. Such a large reduction in the out-of-plane lattice parameter is likely to be the result of both $\langle M-O \rangle$ bond length reduction and an increase of octahedral rotation. This shrinkage is much larger than is

realized in BLMO (only 1%).²⁹ As a result, also the pseudocubic unit cell volume of BSMO is much smaller than undoped BMO and BLMO, 58.8 ± 0.02, 60.5 ± 0.02, and 60.1 Å³ respectively, suggesting strong 3D chemical pressure in BSMO. For BSMO, two peaks were observed along the out-of-plane direction (Figure 1a and b), which indicate d -spacings of 3.87 ± 0.01 Å and 3.83 ± 0.01 Å. We used the lower angle peak (of higher intensity peak) for the out-of-plane lattice parameter (3.83 ± 0.01 Å) because the c-axis oriented phase was the dominant phase seen by cross-sectional TEM. The presence of two peaks can be explained by twinning of the BSMO, which is discussed in more detail later.

Figure 1c compares ω -rocking curves of BSMO with BMO, with $\Delta\omega$ of 0.24° and 0.35°, respectively. The reduction in $\Delta\omega$ indicates less out-of-plane tilting in the BSMO films, which can be explained by higher phase purity. Figure 1d shows φ -scans of the (110) peak of BSMO and the STO. The film peaks have the same peak positions as the STO film indicative of cube-on-cube epitaxy. The alignment (in this case, in-plane rotation) for BSMO ($\Delta\varphi = 0.48^\circ$) is better compared to that of undoped-BMO ($\Delta\varphi = 0.62^\circ$, not shown), again consistent with the higher phase purity and improved growth for BSMO.

Hence, it is clear from the XRD results of Figures 1a–c that Sm substitution promotes BMO phase stabilization and improves the crystallinity. We recall that La-doping gives a stabilizing effect allowing growth of phase pure BLMO films because of the reduction of the destabilizing JT distortion by reducing the amount of Bi in the structure. Here, we have a similar level of Bi content reduction to stabilize the phase, but compared to bulk BMO, we also have a reduction in the lattice parameter to be closer to STO, giving a further stabilization effect.

The AFM height images, shown in Figure 1e and f, confirm the X-ray data. The triangular grains in the undoped-BMO film are likely (00l) oriented Mn₃O₄ (as observed in the θ –2θ scans, Figure 1a). For BSMO (Figure 1f), a homogeneous surface morphology of aligned rectangular faceted grains was observed. The inset of Figure 1f shows twinning domains indicated by white circles. Similar twinning has been observed in perovskite thin films of PbTiO₃ and was thought to arise from the strain relief because of the different lattice parameters of the film and substrate ($a < a_s$, substrate lattice parameter $< c$).^{42,43} The root-mean-square (RMS) roughness for BSMO is ~3 nm, which is

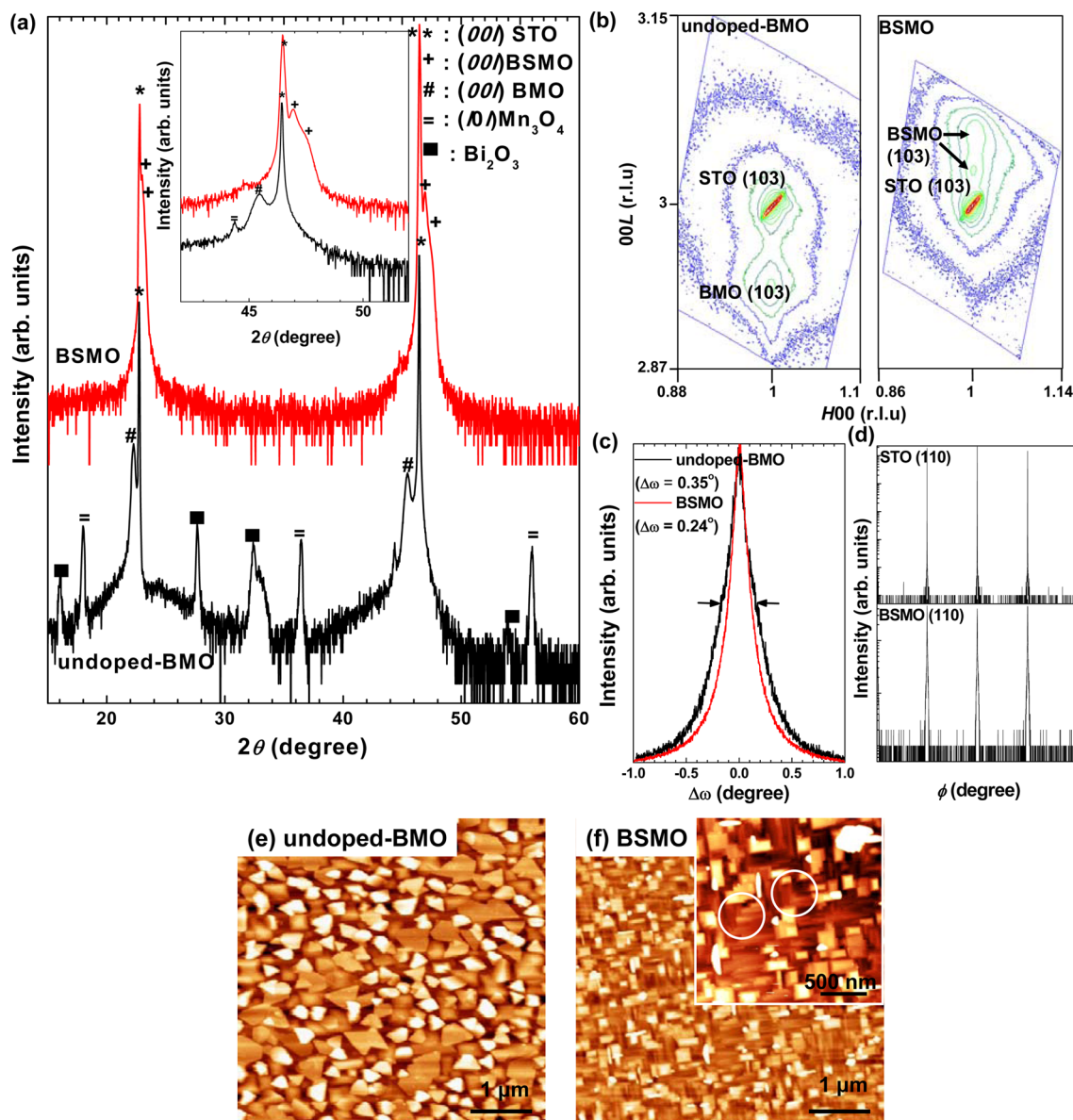


Figure 1. XRD and AFM images. (a) θ - 2θ scans of 200 nm thick undoped-BMO and BSMO films. The inset shows the film (002) peak in detail. (b) RSM around the (103) reflections. (c) ω -rocking curves of the (002) diffraction peak of undoped-BMO (black line) and BSMO (red line) films. (d) 360° ϕ -scan of the (110) reflection of STO substrate (top panel) and the BSMO film (bottom panel). Atomic force microscopy surface topography images of (e) a 200 nm thick undoped-BMO film and (f) a 200 nm thick BSMO film. The inset shows AFM images with $2 \times 2 \mu\text{m}^2$. White circles indicate twinning domains.

much lower than the RMS roughness of 33 nm measured for the undoped-BMO films.

Figure 2a shows a cross-sectional STEM image of a 120 nm thick BSMO film showing high uniformity of composition over a large area.

The sample has many regions of twinned domains as detected in a high resolution cross-sectional TEM (HRTEM) image (Figure 2b), which is in agreement with our XRD results. A clear twin interface is indicated by the dashed line. The presence of twinning in the BSMO films indicates that for bulk BSMO $a_{\text{BSMO}} \neq c_{\text{BSMO}}$ and $a_{\text{BSMO}} < a_{\text{STO}} < c_{\text{BSMO}}$. This would agree with the structure for $\text{Bi}_{1-x}\text{Sr}_x\text{MnO}_3$ with equal cell volume as our BSMO films (58.8 \AA^3).³⁹ In contrast, for undoped BMO, both a_{BMO} and c_{BMO} are larger than a_{STO} , so no twinning is expected.^{39,42,43} The reason that $a_{\text{BSMO}} < a_{\text{STO}} < c_{\text{BSMO}}$ in BSMO may be because of the variation of apical

distance of the MnO octahedra caused by the substitution of a smaller ion than Bi^{3+} .^{35,44,45} Note that a more detailed study should be done to reveal the exact origin of the twinning in BSMO on STO, which is out of the scope of this study. Herein c_{BSMO} is the pseudocubic out-of-plane lattice parameter. The inset of Figure 2b shows an enlarged lattice structure. On the basis of the diffraction pattern and the lattice fringes of the inset of Figure 2c, the unit cell is doubled in the out-of-plane direction. Hence, the structure is (pseudo)-tetragonal with $c \sim 2a$. The doubled cell structure is very similar to that found in $\text{Bi}_{1-x}\text{La}_x\text{FeO}_3$ films ($x = 0.3$) where the doubling is caused by rotation of FeO_6 octahedra.³⁵

Figure 2c shows selected area electron diffraction (SAED) pattern along the STO [010] zone axis. On the basis of the diffraction pattern, the epitaxial relationship between BSMO and STO was found to be [001]BSMO//[001]STO, [100]-

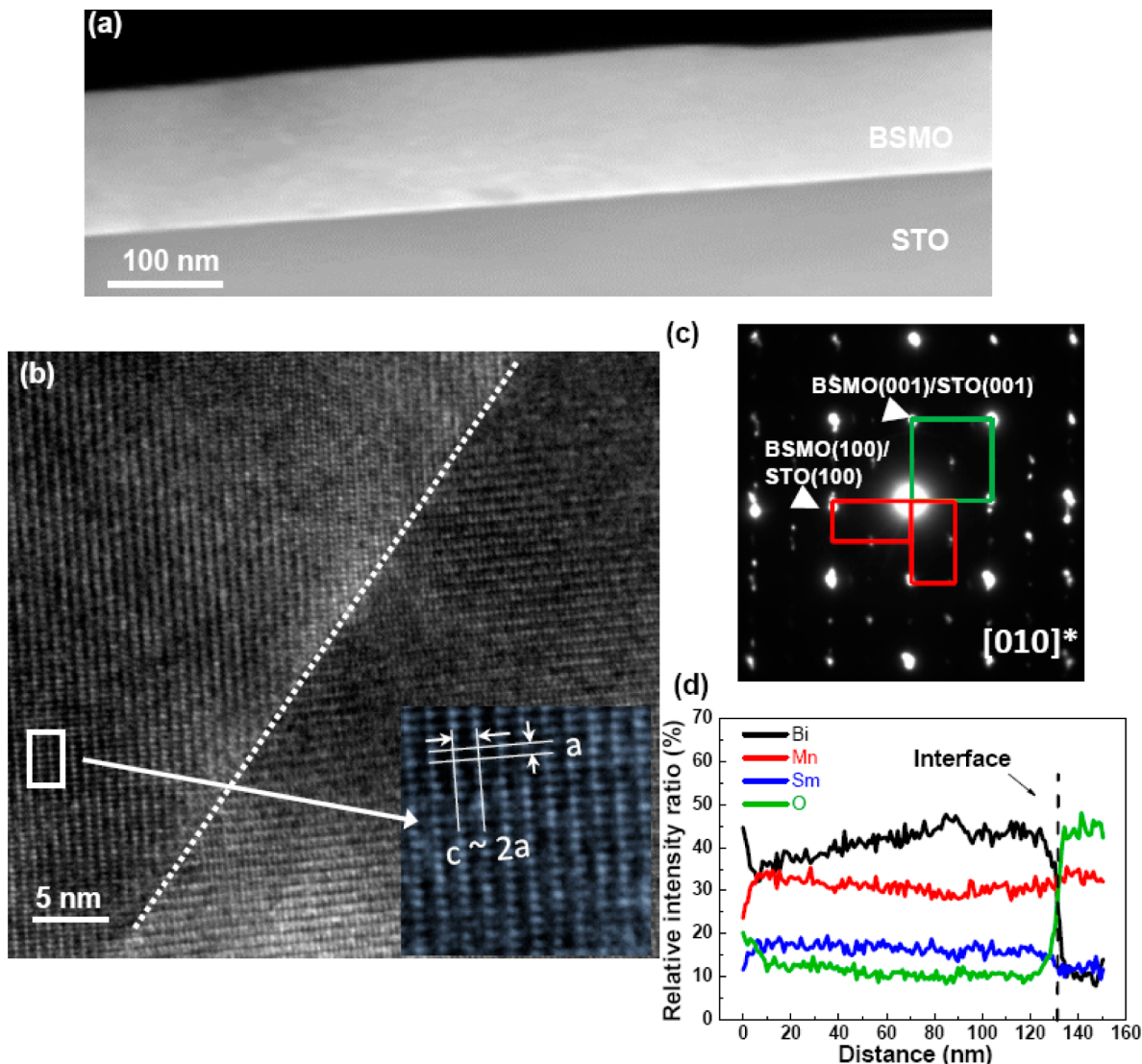


Figure 2. TEM data on BSMO film. (a) Low magnification STEM image of ~ 120 nm thick BSMO on STO. The uniform contrast indicates a homogeneous film composition. (b) High resolution cross-sectional TEM image of a twinned area of BSMO film, where the boundary is indicated by the white dashed line. The inset shows c - and a -axis parameters. (c) SAED patterns of a BSMO film along the $[010]^*$ zone axis. (d) Compositional profiles by EDX line-scans in the TEM through film thickness (0 nm being the top of the film).

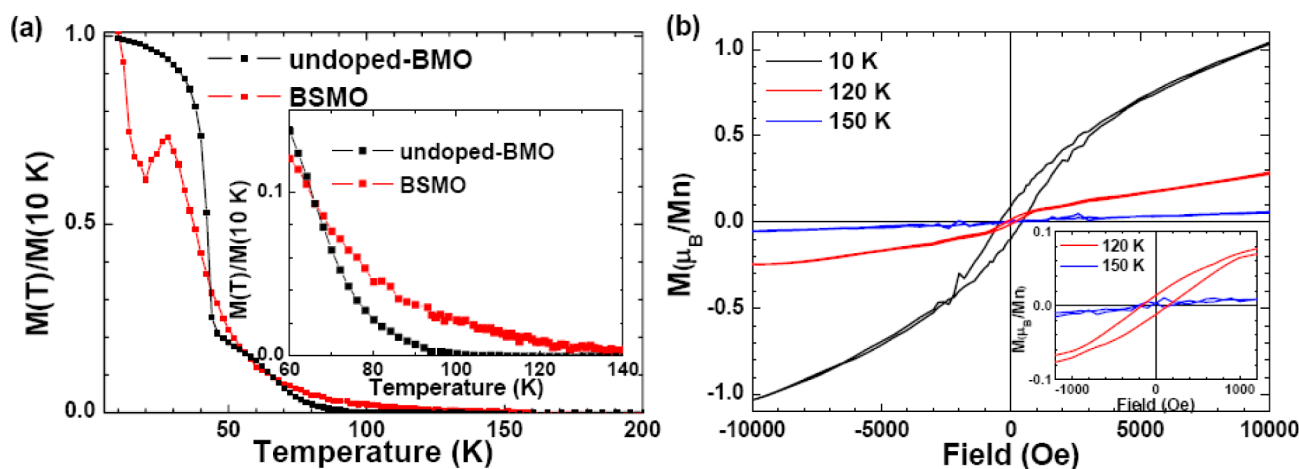


Figure 3. Magnetic properties of 200 nm thick undoped-BMO and BSMO films. (a) The normalized in-plane $M - T$ curve at a field of 200 Oe. (b) Magnetic hysteresis ($M - H$) curves of BSMO in the range of $-10 \leq H \leq 10$ kOe with the field applied in-plane at 10, 120, and 150 K. The inset shows $M - H$ at 120 and 150 K in detail.

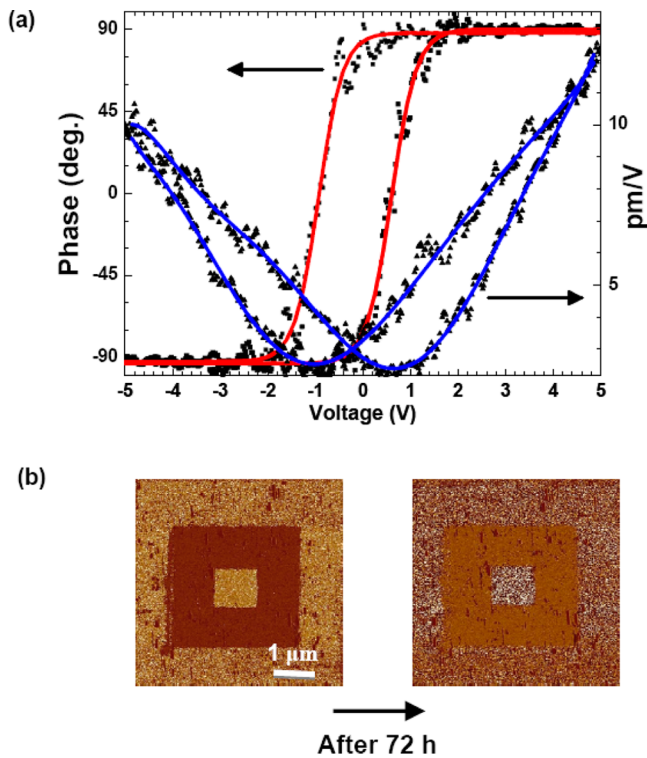


Figure 4. Ferroelectric properties of a 170 nm thick BSMO film on Nb-STO. (a) Amplitude (triangle and blue line) and phase (square and red line) of the PFM signal as a function of bias voltage. (b) PFM phase contrast scan at RT on BSMO after -5 V writing ($5 \times 5\text{ }\mu\text{m}^2$), 5 V rewriting ($3 \times 3\text{ }\mu\text{m}^2$), and -5 V rewriting ($1 \times 1\text{ }\mu\text{m}^2$) at RT, directly after writing (left), and after 72 h (right).

BSMO//[100]STO, and [110]BSMO//[110]STO, consistent with the X-ray data from Figure 1. We show the two twinning orientations of the BSMO crystallites as orthogonal red rectangles.

Energy dispersive X-ray spectroscopy (EDX) line scans were also conducted on the TEM specimen (Figure 2d). An average Sm doping of $x = 0.25$ ($\sim 5\%$ accuracy) was found in the film. This value is higher than the nominal $x = 0.15$ value in the target. The difference can be explained by evaporation of the volatile Bi during growth, which is common during Bi based perovskite film growth.⁴⁶ The filling of Bi vacancies by Sm likely contributes to the observed stabilization of the BSMO films, allowing them to be grown over a wider range of conditions than pure BMO.

Figure 3 compares the magnetic properties of a 200 nm thick undoped-BMO and BSMO films (black and red squares, respectively). In the undoped-BMO film, two FM transitions are present (Figure 3a), one at $\sim 100\text{ K}$ for BMO and the other at $\sim 40\text{ K}$ for Mn_3O_4 , consistent with the phases observed by XRD (Figure 1a). The BSMO film, however, shows two different magnetic transitions, one being an FM transition of as high as $\sim 140\text{ K}$ and the other being an AFM one at $\sim 30\text{ K}$. In addition, the $M - T$ curve of BSMO shows a tail behavior, similar to BMO films reported in the literature.^{14,21,23}

The $M - H$ measurements of BSMO at 10 K showed an M (at 1 T) of $\sim 1.04\text{ }\mu\text{B/Mn}$ and a coercivity (H_C) of 430 Oe (Figure 3b). The H_C of BSMO is in the same range as that for pure BMO and BLMO,^{21,28} while M is significantly higher than that for our undoped-BMO films grown under the same growth conditions ($M = 0.4\text{ }\mu\text{B/Mn}$; see Table 1). To confirm that the

FM transition of BSMO was above 100 K , we measured $M - H$ also at 120 and 150 K (Figure 3b). Clear hysteresis loops were obtained at 120 K with $H_C \sim 130\text{ Oe}$ and $M_r \sim 0.2 M_{r(10K)}$, whereas a paramagnetic hysteresis loop was observed at 150 K (see also inset of Figure 3b). The magnetization of BSMO does not saturate, which is similar to that of pure BMO films and this is likely because of spin canting.²¹ The canting may be due to the competition of hidden AFM and FM ordering.^{8,21,23} Despite the competition of AFM and FM, the magnetic moment value of BSMO at 10 K ($1.04\text{ }\mu\text{B/Mn}$) is higher than that for pure BMO films, which also show FE, and close to the one for BLMO films, $1\text{ }\mu\text{B/Mn}$ (Table 1).^{23,28}

Now, we discuss the possible reason for the enhanced T_C in BSMO. As we have already mentioned, BMO has complex magnetic ordering. There is competition between FM and AFM interactions, with FM interactions out-of-plane and both FM and AFM interactions in-plane.^{13–15} In the case of La^{3+} substitution, when the Bi^{3+} is displaced by the La^{3+} , the JT distortion is decreased, and since La^{3+} has approximately the same size as Bi^{3+} , there is no compensating distortion from the small ion size.⁴⁷ However, in the case of Sm^{3+} , even though there is some Bi^{3+} loss, the JT distortion should be maintained because of the smaller ion size of Sm^{3+} . As we mentioned in the introduction, SmMnO_3 has a JT distortion parameter close to that of BMO. In addition, SmMnO_3 is a canted A-type AFM with a ferrimagnet component in contrast with LMO.⁴⁸ According to theoretical calculations on the relationship between tilting angle of RMnO_3 (R : trivalent lanthanides) and ionic radii, 25% Sm substitution in BMO would lead to a tilting angle that is only slightly increased compared to BMO.⁴⁹ Therefore, we would expect Sm not to destroy the magnetism of BMO like La does. In addition, we expect that besides octahedral rotations, there is also a small decrease of the $\langle \text{Mn}-\text{O} \rangle$ bond length along the out-of-plane axis. The 4% reduction in unit cell volume compared to the pure bulk BMO and the 3% reduction of the out-of-plane lattice parameter (Table 1) are both evidence of this. This is in agreement with the enhancement of FM interactions in the out-of-plane direction, which is expected because of the reduction of the out-of-plane $\langle \text{Mn}-\text{O} \rangle$ bond length.

However, an AFM transition is present at $\sim 30\text{ K}$. In BMO under 1 GPa external hydrostatic pressure, an AFM transition is also observed but at a higher temperature, 90 K .¹¹ Hence, the combined chemical and biaxial pressure in BSMO films is much less detrimental than hydrostatic pressure because the shrinkage of the in-plane lattice parameter is limited by biaxial pressure from substrate.

Hence, through balancing both chemical and biaxial pressure to tune the in-plane and out-of-plane strain independently, it is possible to enhance the FM interaction so that it dominates over the AFM interaction. This is the first time the FM T_C has been increased in BMO by any means. The result naturally leads to the intriguing possibility of whether the growth of BSMO films on a substrate with a larger lattice parameter than STO may further weaken the AFM interactions and strengthen FM ones. Our preliminary results on very thin BSMO films ($\sim 20\text{ nm}$) on $(110)\text{ DyScO}_3$ look promising in terms of magnetic properties, but further work is required to be able to measure the FE properties.

Turning to the ferroelectric properties of the BSMO films on Nb-STO, we show the PFM measurements, amplitude, and phase as a function of bias voltage of a 170 nm thick BSMO film in Figure 4a. After sweeping the DC voltage from $+5$ to -5

to +5 V, a characteristic hysteretic behavior is observed indicative of ferroelectricity at RT. Figure 4b shows the PFM images immediately after poling (left image) and reading again after 72 h (right image). The phase contrast still remains after 72 h. This long retention time is also indicative of ferroelectricity.²² Moreover, the d_{33} of 10 pm/V is higher than previously reported for BLMO films (2 pm/V) at RT.²⁸ As already mentioned, PFM response in pure BMO has only been reported in very thin films (<10 nm), which are coherently strained to give the required structural change to pseudocubic.²² The improved d_{33} is consistent with the enhanced d_{33} reported for Sm doped BiFeO₃ films.^{34–36}

4. CONCLUSIONS

Through a new combined chemical pressure and substrate biaxial pressure crystal engineering approach in thin films, we have demonstrated significantly improved multiferroic properties in BSMO films at the same time as making the growth of phase pure films more facile. The ferromagnetic transition temperature was increased in BSMO by ~40 K to up to 140 K, and the piezoresponse amplitude at room temperature was 10 pm/V, much higher than that reported previously in any BMO film. More broadly, simultaneous tuning of chemical pressure and biaxial substrate pressure represents a very promising new avenue to precisely control the 3D strain state in a large number of other strongly correlated transition metal oxides where the physical properties are extremely dependent on bond lengths and angles in the different crystallographic directions.

■ AUTHOR INFORMATION

Corresponding Author

*E-mail: emc63@cam.ac.uk.

Author Contributions

J.L.M.D. and E.M.C. designed and organized this work. E.M.C. and O.J.L. fabricated films. E.M.C measured the magnetic properties. E.M.C., O.J.L., and J.E.K analyzed the crystal structure of the films using X-ray diffraction. A.C., W.Z., and H.W. carried out high resolution transmission electron microscopy. A.K. carried out piezoresponse force microscopy measurements. E.M.C., J.E.K., and J.L.M.D. wrote the manuscript.

Notes

The authors declare no competing financial interest.

■ ACKNOWLEDGMENTS

This research was funded by the Engineering and Physical Sciences Research Council (EP/P50385X/1) and the European Research Council (ERC-2009-AdG 247276 NOVOX). The TEM work at Texas A&M University was funded by the U.S. National Science Foundation (DMR-1007969 and DMR-1401266).

■ REFERENCES

- (1) Hill, N. A. Why Are There so Few Magnetic Ferroelectrics? *J. Phys. Chem. B* **2000**, *104*, 6694–6709.
- (2) Bibes, M.; Barthélémy, A. Multiferroics: Towards a Magnetoelectric Memory. *Nat. Mater.* **2008**, *7*, 425–426.
- (3) Velev, J. P.; Duan, C.-G.; Burton, J. D.; Smogunov, A.; Niranjan, M. K.; Tosatti, E.; Jaswal, S. S.; Tsymbal, E. Y. Magnetic Tunnel Junctions with Ferroelectric Barriers: Prediction of Four Resistance States from First Principles. *Nano Lett.* **2009**, *9*, 427–432.
- (4) Velev, J. P.; Jaswal, S. S.; Tsymbal, E. Y. Multi-ferroic and Magnetoelectric Materials and Interfaces. *Philos. Trans. R. Soc., A* **2011**, *369*, 3069–3097.
- (5) Moreira dos Santos, A.; Parashar, S.; Raju, A. R.; Zhao, Y. S.; Cheetham, A. K.; Rao, C. N. R. Evidence for the Likely Occurrence of Magnetoferroelectricity in the Simple Perovskite, BiMnO₃. *Solid State Commun.* **2002**, *122*, 49–52.
- (6) Seshadri, R.; Hill, N. A. Visualizing the Role of Bi 6s “Lone Pairs” in the Off-Center Distortion in Ferromagnetic BiMnO₃. *Chem. Mater.* **2001**, *13*, 2892–2899.
- (7) Belik, A. A. Polar and Nonpolar Phases of BiMO₃: A Review. *J. Solid State Chem.* **2012**, *195*, 32–40.
- (8) Solovyev, I. V.; Pchelkina, Z. V. Magnetic-Field Control of the Electric Polarization in BiMnO₃. *Phys. Rev. B* **2010**, *82*, 094425.
- (9) Belik, A. A.; Iikubo, S.; Yokosawa, T.; Kodama, K.; Igawa, N.; Shamoto, S.; Azuma, M.; Takano, M.; Kimoto, K.; Matsui, Y.; Takayama-Muromachi, E. Origin of the Monoclinic-to-Monoclinic Phase Transition and Evidence for the Centrosymmetric Crystal Structure of BiMnO₃. *J. Am. Chem. Soc.* **2007**, *129*, 971.
- (10) Pinsard-Gaudart, L.; Rodríguez-Carvajal, J.; Daoud-Aladine, A.; Goncharenko, I.; Medarde, M.; Smith, R. I.; Revcolevschi, A. Stability of the Jahn-Teller Effect and Magnetic Study of LaMnO₃ under Pressure. *Phys. Rev. B* **2001**, *64*, 064426.
- (11) Kozlenko, D. P.; Belik, A. A.; Kichanov, S. E.; Mirebeau, I.; Sheptyakov, D. V.; Strässle, Th.; Makarova, O. L.; Belushkin, A. V.; Savenko, B. N.; Takayama-Muromachi, E. Competition between Ferromagnetic and Antiferromagnetic Ground States in Multiferroic BiMnO₃ at High Pressures. *Phys. Rev. B* **2010**, *82*, 014401.
- (12) Atou, T.; Chiba, H.; Ohoyama, K.; Yamaguchi, Y.; Syono, Y. Structure Determination of Ferromagnetic Perovskite BiMnO₃. *J. Solid State Chem.* **1999**, *145*, 639–642.
- (13) Moreira Dos Santos, A.; Cheetham, A. K.; Atou, T.; Syono, Y.; Yamaguchi, Y.; Ohoyama, K.; Chiba, H.; Rao, C. N. R. Orbital Ordering as the Determinant for Ferromagnetism in Biferroic BiMnO₃. *Phys. Rev. B* **2002**, *66*, 064425.
- (14) Yang, C.-H.; Koo, T. Y.; Lee, S.-H.; Song, C.; Lee, K.-B.; Jeong, Y. H. Orbital Ordering and Enhanced Magnetic Frustration of Strained BiMnO₃ Thin Films. *Europhys. Lett.* **2005**, *74*, 348.
- (15) Meskine, H.; König, H.; Satpathy, S. Orbital Ordering and Exchange Interaction in the Manganites. *Phys. Rev. B* **2001**, *64*, 094433.
- (16) Bloch, D. The 103 Law for the Volume Dependence of Superexchange. *J. Phys. Chem. Solids* **1966**, *27*, 881.
- (17) Montanari, E.; Righi, L.; Calestani, G.; Migliori, A.; Gilioli, E.; Bolzoni, F. Room Temperature Polymorphism in Metastable BiMnO₃ Prepared by High-Pressure Synthesis. *Chem. Mater.* **2005**, *17*, 1765–1773.
- (18) Toulemonde, P.; Darie, C.; Goujon, C.; Legendre, M.; Mendonca, T.; Alvarez-Murga, M.; Simonet, V.; Bordet, P.; Bouvier, P.; Kreisel, J.; Mezouar, M. Single Crystal Growth of BiMnO₃ under High Pressure-High Temperature. *High Pressure Res.* **2009**, *29*, 600–604.
- (19) Langenberg, E.; Varela, M.; García-Cuenca, M. V.; Ferrater, C.; Sánchez, F.; Fontcuberta, J. Thin Films in Ternary Bi-Mn-O System Obtained by Pulsed Laser Deposition. *Mater. Sci. Eng., B* **2007**, *144*, 138–142.
- (20) Son, J. Y.; Kim, B. G.; Kim, C. H.; Cho, J. H. Writing Polarization Bits on the Multiferroic BiMnO₃ Thin Film using Kelvin Probe Force Microscope. *Appl. Phys. Lett.* **2004**, *84*, 4971.
- (21) Gajek, M.; Bibes, M.; Barthélémy, A.; Bouzehouane, K.; Fusil, S.; Varela, M.; Fontcuberta, J.; Fert, A. Spin Filtering through Ferromagnetic BiMnO₃ Tunnel Barriers. *Phys. Rev. B* **2005**, *72*, 020406.
- (22) De Luca, G. M.; Preziosi, D.; Chiarella, F.; Di Capua, R.; Gariglio, S.; Lettieri, S.; Salluzzo, M. Ferromagnetism and Ferroelectricity in Epitaxial BiMnO₃ Ultra-thin Films. *Appl. Phys. Lett.* **2013**, *103*, 062902.

- (23) Jeen, H.; Singh-Bhalla, G.; Mickel, P. R.; Voigt, K.; Morien, C.; Tongay, S.; Hebard, A. F.; Biswas, A. Growth and Characterization of Multiferroic BiMnO_3 Thin Films. *J. Appl. Phys.* **2011**, *109*, 074104.
- (24) Yang, H.; Chi, Z. H.; Jiang, J. L.; Feng, W. J.; Dai, J. F.; Jin, C. Q.; Yu, R. C. Is Ferroelectricity in BiMnO_3 Induced by Superlattice? *J. Mater. Sci.* **2008**, *43*, 3604.
- (25) Son, J. Y.; Shin, Y.-H. Multiferroic BiMnO_3 Thin Films with Double SrTiO_3 Buffer Layers. *Appl. Phys. Lett.* **2008**, *93*, 062902.
- (26) Grizalez, M.; Mendoza, G. A.; Prieto, P. Analysis of Multiferroic Properties in BiMnO_3 Thin Films. *J. Phys. Conf. Ser.* **2009**, *167*, 012035.
- (27) Troyanchuk, I. O.; Mantytskaja, O. S.; Szymczak, H.; Shvedun, M. Yu. Magnetic Phase Transitions in the System $\text{La}_{1-x}\text{Bi}_x\text{MnO}_{3+\lambda}$. *Low Temp. Phys.* **2002**, *28*, 569.
- (28) Gajek, M.; Bibes, M.; Fusil, S.; Bouzehouane, K.; Fontcuberta, J.; Barthélémy, A.; Fert, A. Tunnel Junctions with Multiferroic Barriers. *Nat. Mater.* **2007**, *6*, 296–302.
- (29) Gajek, M.; Bibes, M.; Wyczisk, F.; Varela, M.; Fontcuberta, J.; Barthélémy, A. Growth and Magnetic Properties of Multiferroic $\text{La}_x\text{Bi}_{1-x}\text{MnO}_3$ Thin Films. *Phys. Rev. B* **2007**, *75*, 174417.
- (30) Kimura, T.; Kawamoto, S.; Yamada, I.; Azuma, M.; Takano, M.; Tokura, Y. Magnetocapacitance Effect in Multiferroic BiMnO_3 . *Phys. Rev. B* **2003**, *67*, 180401(R).
- (31) Sugawara, F.; Iida, S.; Syono, Y.; Akimoto, S.-I. Magnetic Properties and Crystal Distortions of BiMnO_3 and BiCrO_3 . *J. Phys. Soc. Jpn.* **1968**, *25*, 1553.
- (32) Jia, Y. Q. Crystal Radii and Effective Ionic Radii of the Rare Earth Ions. *J. Solid State Chem.* **1991**, *95*, 184–187.
- (33) Maris, G.; Volotchaev, V.; Palstra, T. T. M. Effect of Ionic Size on the Orbital Ordering Transition in $\text{RMnO}_{3+\delta}$. *New J. Phys.* **2004**, *6*, 153.
- (34) Kan, D.; Pálová, L.; Anbusathaiah, V.; Cheng, C. J.; Fujino, S.; Nagarajan, V.; Rabe, K. M.; Takeuchi, I. Universal Behavior and Electric-Field-Induced Structural Transition in Rare-Earth-Substituted BiFeO_3 . *Adv. Funct. Mater.* **2010**, *20*, 1108–1115.
- (35) Kan, D.; Cheng, C.-J.; Nagarajan, V.; Takeuchi, I. Composition and Temperature-Induced Structural Evolution in La, Sm, and Dy Substituted BiFeO_3 Epitaxial Thin Films at Morphotropic Phase Boundaries. *J. Appl. Phys.* **2011**, *110*, 014106.
- (36) Singh, S. K.; Tomy, C. V.; Era, T.; Itoh, M.; Ishiwara, H. Improved Multiferroic Properties in Sm-doped BiFeO_3 Thin Films Deposited using Chemical Solution Deposition Method. *J. Appl. Phys.* **2012**, *111*, 102801.
- (37) Cheng, C.-J.; Kan, D.; Anbusathaiah, V.; Takeuchi, I.; Nagarajan, V. Microstructure-Electromechanical Property Correlations in Rare-Earth-Substituted BiFeO_3 Epitaxial Thin Films at Morphotropic Phase Boundaries. *Appl. Phys. Lett.* **2010**, *97*, 212905.
- (38) Shin, H.; Song, J.-T. Piezoelectric Coefficient Measurement of AlN Thin Films at the Nanometer Scale Using Piezoresponse Force Microscopy. *JKPS* **2010**, *56*, 580–585.
- (39) Chiba, H.; Atou, T.; Syono, Y. Magnetic and Electrical Properties of $\text{Bi}_{1-x}\text{Sr}_x\text{MnO}_3$: Hole-Doping Effect on Ferromagnetic Perovskite BiMnO_3 . *J. Solid State Chem.* **1997**, *132*, 139.
- (40) JCPDS no. 35-0734.
- (41) Shannon, R. D.; Prewitt, C. T. Effective Ionic Radii in Oxides and Fluorides. *Acta Crystallogr., Sect. B* **1969**, *25*, 925–946.
- (42) Vlooswijk, A. H. G. Structure and Domain Formation in Ferroelectric Thin Films. Ph.D. Thesis, The University of Groningen, June 2009.
- (43) Catalan, G.; Lubk, A.; Vlooswijk, A. H. G.; Snoeck, E.; Magen, C.; Janssens, A.; Rispens, G.; Rijnders, G.; Blank, D. H. A.; Noheda, B. Flexoelectric Rotation of Polarization in Ferroelectric Thin Films. *Nat. Mater.* **2011**, *10*, 963–967.
- (44) Motin Seikh, Md.; Pralong, V.; Lebedev, O. I.; Caaignaert, V.; Raveau, B. The Ordered Double Perovskite $\text{PrBaCo}_2\text{O}_6$: Synthesis, Structure, and Magnetism. *J. Appl. Phys.* **2013**, *114*, 013902.
- (45) MacLaren, I.; Wangad, Z. L.; Wang, H. S.; Lib, Q. The Effects of Film-substrate Mismatch on $\text{Pr}_{0.7}\text{Ca}_{0.3}\text{MnO}_3$ Thin Films. *Philos. Mag. A* **2002**, *82*, 1405–1417.
- (46) Béa, H.; Bibes, M.; Fusil, S.; Bouzehouane, K.; Jacquet, E.; Rode, K.; Bencok, P.; Barthélémy, A. Investigation on the Origin of the Magnetic Moment of BiFeO_3 Thin Films by Advanced X-ray Characterizations. *Phys. Rev. B* **2006**, *74*, 020101(R).
- (47) Tachibana, M.; Shimoyama, T.; Kawaji, H.; Atake, T.; Atake, E. Jahn-Teller Distortion and Magnetic Transitions in Perovskite RMnO_3 ($\text{R}=\text{Ho}, \text{Er}, \text{Tm}, \text{Yb}$, and Lu). *Phys. Rev. B* **2007**, *75*, 144425.
- (48) Jung, J.-S.; Iyama, A.; Nakamura, H.; Mizumaki, M.; Kawamura, N.; Wakabayashi, Y.; Kimura, T. Magnetocapacitive Effects in the Néel N-type Ferrimagnet SmMnO_3 . *Phys. Rev. B* **2010**, *82*, 212403.
- (49) Zhou, J.-S.; Goodenough, J. B. Universal Octahedral-Site Distortion in Orthorhombic Perovskite Oxides. *Phys. Rev. Lett.* **2005**, *94*, 065501.